Hindawi
Scientific Programming
Volume 2021, Article ID 2285884, 9 pages
https://doi.org/10.1155/2021/2285884

Research Article

Intelligent Algorithms-Based CT Image Segmentation in Patients with Cardiovascular Diseases and Realization of Visualization Algorithms

Xianhua Huang

Department of Cardiology, The First People's Hospital of Tonglu County, Tonglu 311500, Hangzhou, China

Correspondence should be addressed to Xianhua Huang; 14307080017@fudan.edu.cn

Received 8 July 2021; Revised 14 August 2021; Accepted 16 August 2021; Published 9 September 2021

Academic Editor: Gustavo Ramirez

The study focused on the intelligent algorithms-based segmentation of computed tomography (CT) images of patients with cardiovascular diseases (CVD) and the realization of visualization algorithms. The first step was to design a method for precise segmentation under the cylinder model based on the coronary body data of the coarse segmentation, and then the principles of different visualization algorithms were discussed. The results showed that the precise segmentation method can effectively eliminate most of the branches and calcified lesions; curved planar reformation (CPR) and straightened CPR can display the entire blood vessel on one image; and spherical CPR can display the complete coronary artery tree on an image, so that a problem with a certain blood vessel can be quickly found. In conclusion, the precise segmentation of CT images of CVD and visualization algorithm based on the cylinder model have clinical significance in the diagnosis of CVD.

1. Introduction

Cardiovascular and cerebrovascular diseases, such as stroke and ischemic heart disease, are the leading cause of death in China [1]. According to the China CVD report 2018 released by the Cardiovascular Disease Center [2], the prevalence of cardiovascular diseases (CVD) in China is showing an increasing trend. It is inferred that an estimated 290 million population suffer from CVD, including 13 million with strokes, 11 million with coronary heart disease, and 245 million with hypertension. Coronary heart disease is a CVD. Due to calcification and fat accumulation, plaques are formed in vessels, resulting in irreversible myocardial damage and finally narrowing of the vascular cavity. Coronary artery stenosis can induce myocardial infarction, but early detection can effectively prevent coronary heart disease.

In recent years, with the popularization of medical images in clinical diagnosis and treatment, the research of intelligent algorithms for image segmentation has gradually attracted much attention. Jonathan Long designed a fully voluntary network (FCN) [3] structure, which successfully used deep learning in semantic segmentation. For medical images, Olaf Ronneberger and others put forward a network structure called u-net [4], which is often used in image segmentation in medicine. Ahmed Abdulkadir and others applied u-net to 3D space [5], designed 3D u-net under 3D convolution, and used it in 3D image segmentation. Kuan-Lun Tseng et al. designed a way to associate the upper and lower information of the third dimension, which is called Conv-LSTM [6]. Among the traditional methods, T. Buelow et al. designed a method to segment pulmonary artery, which was propagated forward based on artificial seeding [7], but it was impossible to achieve automatic segmentation. Coronary CT angiography (CTA) is a rapid and low-cost diagnostic method widely used in clinic nowadays [8]. CTA has high sensitivity and negative predictive value, and it is one of the main noninvasive ways to check coronary artery disease [9]. However, CTA has a large amount of data and contains a lot of information, so understanding its images requires doctors to have rich clinical experience. At present, the accuracy of CTA image diagnosis basically depends on

visualization technology. Some studies have shown that visualization technology can observe the places that are not easy to observe in medical images, so it is of great significance in medical education, clinical diagnosis, and surgical navigation [10, 11]. Accurate visualization can be realized according to the accurate segmentation of coronary artery. The so-called image segmentation specifically refers to the separation of interested and relatively valuable objects when processing related images. This technical means is an extremely key technology applied to image processing [12].

2. Experimental Principles and Methods

2.1. Accurate Segmentation of Blood Vessels Based on Intelligent Algorithms

2.1.1. Straightening Volume Data Generation. Straightened CPR is a CPR algorithm, which is mainly used to eliminate the bending of the space structure in the lumen and straighten its structure, to get the three-dimensional data of the lumen. On the one hand, the state of the straightened blood vessel and the changes are displayed completely, and the length of the blood vessel can determine the height of the image. On the other hand, it can also display the cross section of the blood vessel, reflecting the condition of the blood vessel lumen. The method is mainly to input the center line of the blood vessel and establish a coordinate system at each point to prevent the cross section rotating. Otherwise, it will cause image misalignment. The rotation minimizing frame (RMF) [13] is used to construct the coordinate system.

2.1.2. Accurate Segmentation of Blood Vessels Based on Cylinder Model. The condition of the blood vessel, such as stenosis and normality, can be reflected by the cross section of the blood vessel. To accurately segment the cross section of the blood vessel can get the blood flow channel, and then the size of the lumen is measured by the area of the lumen and the degree of diameter stenosis.

In this study, a method for precise segmentation of coronary lumens is designed. The flow chart of this algorithm is shown in Figure 1.

The lumen segmentation is performed layer by layer. The segmentation process of each layer is shown in Figure 2, and there are constraints between two adjacent layers.

2.1.3. Principle of Calcification Detection. Generally, the CT value of blood vessels is greater than 0 HU, and calcified lesions have a large CT value. According to the gray histogram and cumulative histogram of the data in the experiment, it is noted that the frequency of the cumulative histogram of the calcification data can be 1 only when it has a high gray value (usually greater than 700). The cumulative histogram of the calcification data with little or no calcification does not have long tails. Figure 3 shows the data without calcification, and Figure 4 shows the data with calcification. The Ader cumulative histogram has a long tail. The histograms (Figures 5 and 6) show double peaks, and

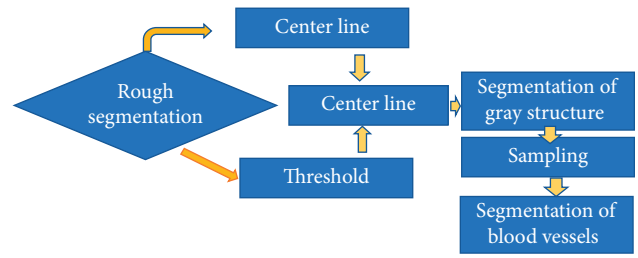

Figure 1: The flow chart of the coronary segmentation algorithm.

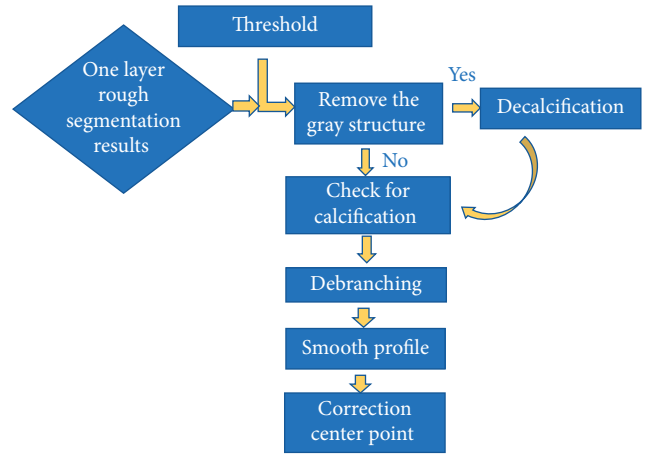

Figure 2: Single-layer segmentation process of the lumen segmentation algorithm.

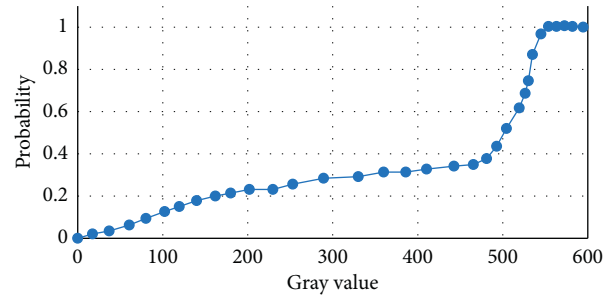

Figure 3: Cumulative histogram of data without calcification.

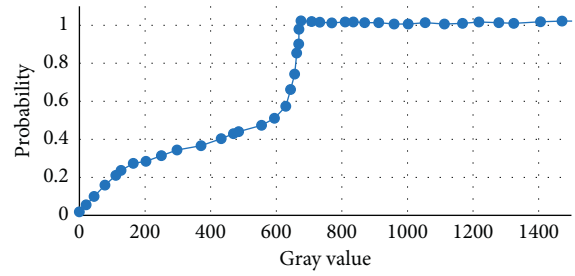

Figure 4: Cumulative histogram of data with calcification.

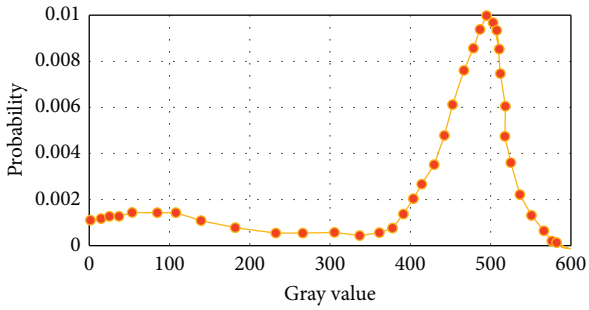

Figure 5: Curve graph of data without calcification.

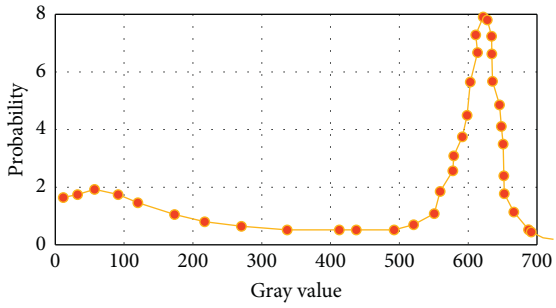

Figure 6: Curve graph of data with calcification.

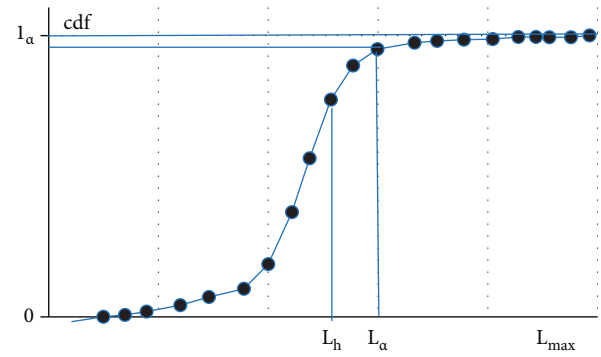

Figure 7: Curve graph of the CT values greater than 0 HU.

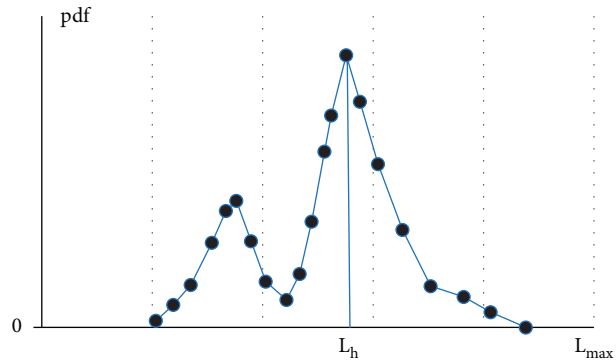

Figure 8: Curve graph of the CT values greater than 0 HU.

only the CT values higher than 0 HU are included. Based on this, a method to inspect and remove calcification is proposed.

Figures 7 and 8 are gray histogram and cumulative histogram of the CT values higher than 0 HU. If CT value $L_{\max} - L_h > 500$ HU, there is calcification. The threshold method is used to remove calcification. The calcification threshold is set as follows.

$$T_{c\alpha} = L_h + (L_\alpha - L_h), \tag{1}$$

where the CT value corresponding to L_h in the histogram is the maximum value, L_α is the CT value of the cumulative histogram $\alpha \in [0, 1]$, and the empirical value is $\alpha = 0.990$.

2.1.4. Debranching and Contour Smoothing. There are often branches in blood vessels, so they need to be removed in the process of evaluating lumen stenosis to facilitate accurate statistics of lumen area. The principle of branch removal is to treat blood vessels as cylinders to achieve branch removal. The general workflow of the branching algorithm is as follows. First, the boundary points of the blood vessel contour are extracted. Then, the distance between the boundary point and the center point is calculated and sorted. Next, the threshold is calculated based on the top 10% of the mean minimum distance. Finally, the threshold is used to clear clean branches.

Due to the existence of lesions, the contour of the lumen presents a nonstandard round shape, so it is constrained by roundness of the shape and the difference in the areas of adjacent layers. In this study, roundness is defined as the ratio of the area of the circle with the same diameter of the long axis of the connected domain to the area of the connected domain; namely,

$$\text{Roundness} = \frac{4A}{\pi L_{\max}^2}, \tag{2}$$

where A is the area of the connected domain, $L_{\max}$ is the length of the major axis of the ellipse equivalent to the connected domain, and the range of roundness is (0, 1]. Smoothing is similar to debranching, but it has a smaller area difference, and the threshold is 8 voxels.

2.1.5. Center Point Prediction. The accuracy of lumen segmentation determines the result of debranching. Therefore, only the voxel with the largest gray value is included in the experiment. The convex combination is sued to finally get the center point of the current layer.

$$A_i = K_1 A_{gi} + K_2 A_{i-1} + (1 - K_1 - K_2) A_{i-1}, \tag{3}$$

where K_1 and K_2 are nonnegative and A_{gi} represents the central point value of the layer obtained by only calculating the gray value.

2.2. Visualization of Coronary Artery CPR. The purpose of the CPR is to highlight the tubular structure on an image. Since the three-dimensional points of the structure are

reflected by the center line, data presentation depends on the center line of the lumen.

2.2.1. The Principle and Realization of Extended CPR. In extended CPR, the direction of interest is a straight line of the cylinder, and its alignment is obtained by mapping the center line. After unfolding the cylinder, the original data is sampled to obtain the extended CPR image (Figure 9).

Generally speaking, maintaining the original structural characteristics of the object in medical images, such as shape and size, is needed. Therefore, when the alignment of the object is straightened, the curve will be sampled according to the same spacing method, and each line of the image will have corresponding sampling points. Then, sampling is performed, and trilinear interpolation is often used.

Sampling of the reference center point: the projection point and the center point correspond to each other after sampling, and the projection point is first sampled and then estimated. If the original center line is $\{\text{Ai}=(x\text{i}, y\text{i}, z\text{i})|i = 1, 2,..., N_{0}\}$, $\{\text{Ci}\}$ is projected along the direction of interest to obtain the projection point set $\{\text{Ki}\}$. In order to obtain the point set $\{P_j = (X\text{i}, Y\text{i}, Z\text{i})|j = 1, 2,..., N\}$, the projection point set is sampled at equal intervals according to the arc length. Each straight line of the original data passing through the point P_j is parallel to the direction of interest, and then the result image is produced. In order to obtain the gray value of the final CPR, the critical point P_j $(j = 1, 2,..., N)$ is used to compare with the reference center point Aj $(j = 1, 2, \ldots, N)$. Because $\widehat{A_j}$ may not be available, P_j is needed to estimate it; namely,

$$\widehat{A_j} = \alpha A_m + (1 - \alpha)A_n. \tag{4}$$

As shown in Figure 10, $\widehat{A_j}$ compares with the sampling projection point P_j, and it is found that the points F_m and F_n with the shortest distance from the point P_j in $\{K_j\}$ compare with A_m and A_m. If these two points are placed on both sides of P_j, there is

$$\alpha = \frac{\left|\overrightarrow{P_jF_n}\right|}{\left|\overrightarrow{F_mF_n}\right|}. \tag{5}$$

If they are all distributed on the same side of P_j and F_m is the closest, then

$$\widehat{A_j} = \frac{\left(\left|\overrightarrow{F_nF_m}\right|A_n + \left|\overrightarrow{F_nP_j}\right|\overrightarrow{F_nF_m}\right)}{\left|\overrightarrow{F_nF_m}\right|}. \tag{6}$$

Because the number of projection points is equal to the height of the generated image after sampling, the height of the generated image is associated with the direction of interest and the structure of the blood vessel. A more curved blood vessel indicates a lower height of the generated image.

Gray interpolation: the generated image is obtained by unfolding the guideline of its cylinder. Usually, a heart CTA is square with 512×512 pixels, so the width of the extended CPR image should also be 512, that is, the diameter of the largest inscribed circle, so the generated image is only displayed within the largest inscribed circle. For projection, the offset on one side of the center point is calculated first, and then the offset on the other side is calculated according to the calculated offset. The image width and projection vector are expressed by W and v, and then the three-dimensional coordinates of Δx at jth line are

$$A = \widehat{A}_j + v\Delta x, \tag{7}$$

where A_j is the estimated reference center point for the jth row.

Trilinear interpolation is used for grayscale interpolation. Figure 11 shows the trilinear interpolation. The point $P(a, b, c)$ is located in a cube. The downward and upward coordinate components are rounded and expressed as a_L and a_h, respectively. At the same time, the b and c components are rounded to achieve trilinear interpolation. First, interpolation is performed in the b direction. With Q_4 as an example, the equation is shown below:

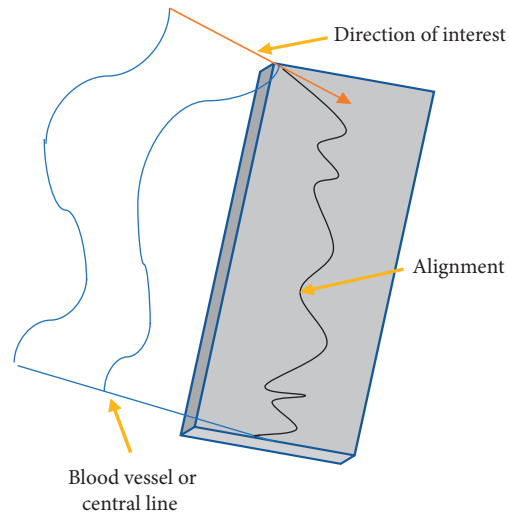

Figure 9: Sampling surface of extended CPR.

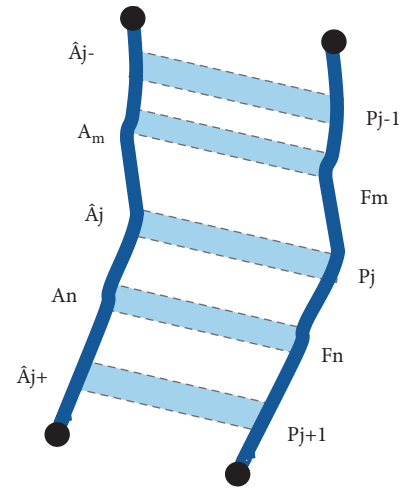

Figure 10: The estimated center point of the projected point in extended CPR.

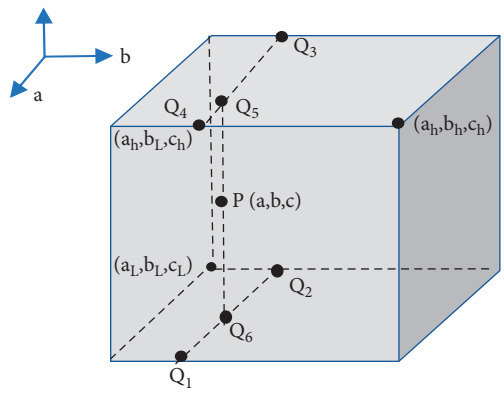

Figure 11: Principle of trilinear interpolation.

$$Q_4 = (b_h - b)I(a_h\ ,\ b_L\ ,\ c_h) + (b - b_L)I(a_h\ ,\ b_h, c_h). \quad (8)$$

In the same way, Q1∽Q3 are obtained. Then, linear interpolation is performed in the x direction, and the following equation is obtained:

$$\begin{aligned} Q_5 &= (a_h - a)Q_4 + (a - a_L)Q, \\ Q_6 &= (a_h - a)Q_1 + (a - a_L)Q_3. \end{aligned} \quad (9)$$

Next, linear interpolation is performed in the z direction to get the grayscale at point P.

$$Q_0 = (c_h - c)Q_6 + (c - c_L)Q_5. \quad (10)$$

The coordinates corresponding to the center line of the generated image are the key to obtaining extended CPR. With the coordinates as a reference point, the offset is calculated, and then the volume data coordinates of all points are calculated according to the direction of interest. The implementation process of extended CPR is as follows, including three parts. First, the coordinates of the center point after projection are obtained; then, the sampling point of the center point is obtained according to the interpolation, and the gray sampling point of the generated image is the center point of interpolation estimation; finally, gray interpolation is performed.

The three-dimensional volume coordinates obtained are projected into the coordinates of the generated image, and then the grayscale interpolation is performed according to the two-dimensional coordinates. Assuming that the point set of the original center point is $\{A_{i1}= (a_i,b_i, c_i)|i = 1, 2, \ldots, N_0\}$, the previous point and the center point are set to A_{i-1} and A_i. The direction of interest is set to $v= (\cos\theta, \sin\theta, 0)$, the angle between the $a0b$ two-dimensional plane and $a$axis is θ, and then the center point is projected according to the direction of interest. Then, the following equation is obtained.

$$\begin{cases} \Delta a_i = \overrightarrow{A_{i-1}A_1} \cdot v, \\ \Delta b_i = \sqrt{\left|\left|\overrightarrow{A_{i-1}A_i}\right|\right|^2 - \Delta a^2}. \end{cases} \quad (11)$$

The image coordinates after projection are (xi, y_i), and then the following equation is obtained.

$$\begin{cases} a_i = a_{i-1} + \Delta a_i, \quad a_0 = \dfrac{w}{2}, \\ b_i = b_{I-1} + \Delta b_i, \quad b_0 = 0, \end{cases} \quad (12)$$

where w is the width of the generated image, which is the same width as that of the CT image. In this case, the resulting image is only displayed in the largest inscribed cylinder. For the coordinate set $\{(i,\ bi)|i = 1,\ 2,...,N_0\}$ of the generated image, the equidistant sampling is performed according to the y component, to obtain a new point set $\{(\hat{a}_i,\ \hat{b}_i)|i = \hat{a}_i 1,\ 2,..., N\}$. Each point in this point set corresponds to a center point, so a new center point set $\{\hat{A}_i = (a_i, b_i, c_i)|i = 1, 2,..., N\}$ is obtained. The points $(\hat{a}_r,\ \hat{a}_r)$ in the generated image all correspond to the original space coordinates a; namely,

$$a = \hat{A}_j + \left(\hat{a}_r - \frac{w}{2}\right)v. \quad (13)$$

In (13), w represents the width of the generated image, and the gray value of each point is obtained according to trilinear gray interpolation.

2.2.2. Straightened CPR. Straightened CPR removes the curl of the spatial structure and uses linearity to show the change in the diameter of the tubular structure. Therefore, the length of the lumen center line determines the height of the generated image.

The curvature of the imaging plane parallel to the center line can eliminate the tubular structure and describe the spatial curvature and organization information near the curve. There are two methods to generate the local coordinates of the space curve, namely, the Frenet frame (also known as the TNB coordinate system) and the rotation minimizing frame (RMF). They are composed of three mutually perpendicular vectors; the tangent direction of the curve is one of them, and the other two form a plane perpendicular to the tangent vector.

The straightened CPR is realized mainly by finding the local coordinate system according to the center line. There are many ways to turn the center line into the RMF coordinate system. The phase initial vector determines the Frenet coordinate system and the RMF coordinate system. To facilitate the calculation of data, the a-axis or b-axis vector is selected as the reference vector of the initial vector. If the center point set is $\{A_I=(a_i,\ b_ic_i)|\ i = 1,\ 2,..., N\}$, the tangent vector $p_i = ((A_{i=2} - A_I)/2)$ is obtained according to the second-order difference of the center point. The main vector and secondary vector algorithms are as follows:

$$\begin{aligned} n_i &= n_{i-1}(1 - p_{i-1}p_i), \\ b_i &= p \times n_i. \end{aligned} \quad (14)$$

Finally, a vector set of coordinates $\{(p_i, n_i, b_i)\ |i = 1, 2, \ldots, N\}$ is obtained. The coordinate system vector set and the center point are used for grayscale interpolation to obtain straightened data. Assuming that the coordinates of the main vector and the secondary vector of the i-th layer cross section are x_i and y_i, $i = 1,\ 2,\ \ldots,\ N$, the volume data

coordinates corresponding to the gray level at (a_i, b_i) in the cross section are as follows.

$$P = A_i + A_i n_i + B_i b_i. \tag{15}$$

Through trilinear interpolation, volume data is obtained.

2.2.3. Spherical CPR. This method displays the number of blood vessels as much as possible by inputting all the center lines from the coronary artery branches, then obtains the envelope surface of all the center lines, and finally displays the maximum density projection on the spherical surface. The globe form uses the center line to display the grayscale of the real shape on the spherical surface, and most of the blood vessels are distributed near the equator. Mercator projection technology is obtained in the form of a globe.

Heart line envelope calculation: the three main coronary arteries, left anterior descending (LAD) branches, left circumflex (LCX) branches, and right coronary artery (RCA), are input, and the least squares fitting method is used to fit the spherical surface, which can reduce the influence of the small branches of the coronary artery on the fitting result. If the radius of the target sphere is R and the center of the sphere is $A_0(a_0, b_0, c_0)$, there are N center points and the total error of the fitting is as follows.

$$E\left(a_0, b_0, c_0, R\right) = \sum_{i=1}^{N} \left[(a_i - a_0)^2 + (b_i - b_0)^2 + (c_i - c_0)^2 - R^2 \right]^2. \tag{16}$$

Then, partial derivatives of a_0, b_0, c_0, and R are solved to calculate the spherical parameters. The spherical surface is used as the display surface in the globe mode.

For the spherical evolution, the spherical coordinate system can be used to obtain the spherical grid points, and the evolution process is used to adjust these grid points. The principle is to reduce the degree of deviation of the diameter at this point to make the envelope more accurate.

$$\Delta h = \frac{\Delta h_{\max} \left(\theta_{\max} - \alpha\right)}{\theta_{\max}}. \tag{17}$$

Real mode to globe mode: from the real mode to the globe mode, all gray levels have been obtained. An oblique globe mode image is obtained by projecting the gray level of the real shape radially onto the evolved initial spherical deflection plane.

Mercator projection: it is a commonly used tangent cylindrical projection method. There is basically no angular distortion in Mercator projection, but the distortion of the area is very significant, and the distortion is greater when it is closer to the poles, so only the latitudes below 85° are considered. The relationship between the latitude and longitude projection and the cylindrical plane is as follows:

$$\begin{cases} a = R\theta, \\ \\ b = R \ln\left[\tan\left(\dfrac{\pi}{4} + \dfrac{\varphi}{2}\right)\right], \end{cases} \tag{18}$$

where θ represents longitude, φ represents latitude, and both are radians. According to (18), it can be concluded that the output image in the width direction is nonlinear and the distortion is greater when it is closer to the poles.

3. Segmentation Results and Realization of Visualization

3.1. Segmentation Results. In order to verify the segmentation effects of the cylinder model algorithm, the experiment accurately segmented the lumen data containing plaques, such as stents, stenosis, and calcification, and calculated the area of the lumen at the same time. After inputting the center line and the original coronary artery coarse segmentation data, the lesion and the stent can be observed. Figure 12 shows the segmentation results, lumen area, and straightened blood vessels.

3.2. Realization of Visualization

3.2.1. Extended CPR Results. To realize extended CPR, RCA and LAD were reconstructed. Figure 13 shows the extended CPR results corresponding to the center lines LAD and RCA.

3.2.2. Straightened CPR Results. A segment of LAD was selected to straighten the blood vessel, and Figure 14 shows the straightened results by LAD at different angles.

3.2.3. Spherical CPR Results. To realize CPR, the three main coronary arteries of LAD, LCX, and RCA were selected for spherical fitting, and finally the spherical surface was obtained. Next, all the center points were evolved, and the final globe mode is shown in Figure 15.

4. Discussion

The coronary artery is an important organ of the human body, and it provides arterial blood to the myocardium. Its pathological changes can cause certain diseases such as coronary atherosclerosis, which threatens the physical and mental health of human beings. Coronary CT images can clearly show the structure and pathological conditions of the coronary lumen, so they are widely used in the diagnosis, screening, and prognosis of coronary artery diseases [14, 15]. Medical visualization technology is a three-dimensional model. It can spontaneously perform quantitative and qualitative analysis of the target [16], thus providing clearer images and facilitating functional analysis [17]. Yue (2017) studied the relationship between three-dimensional reconstruction and fluid mechanics with the formation and progression of atherosclerotic plates [18]. Guo et al. (2011) used visualization in three-dimensional echocardiography to reconstruct the coronary artery model to assist in the diagnosis of coronary heart disease [19].

This study focused on the precise segmentation of coronary arteries and different 3D reconstruction methods. According to the segmentation results, it can be concluded that the method proposed in this research can effectively

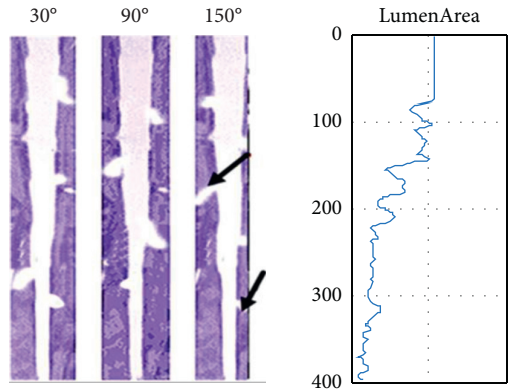

Figure 12: Accurate segmentation results and area calculation results at different angles.

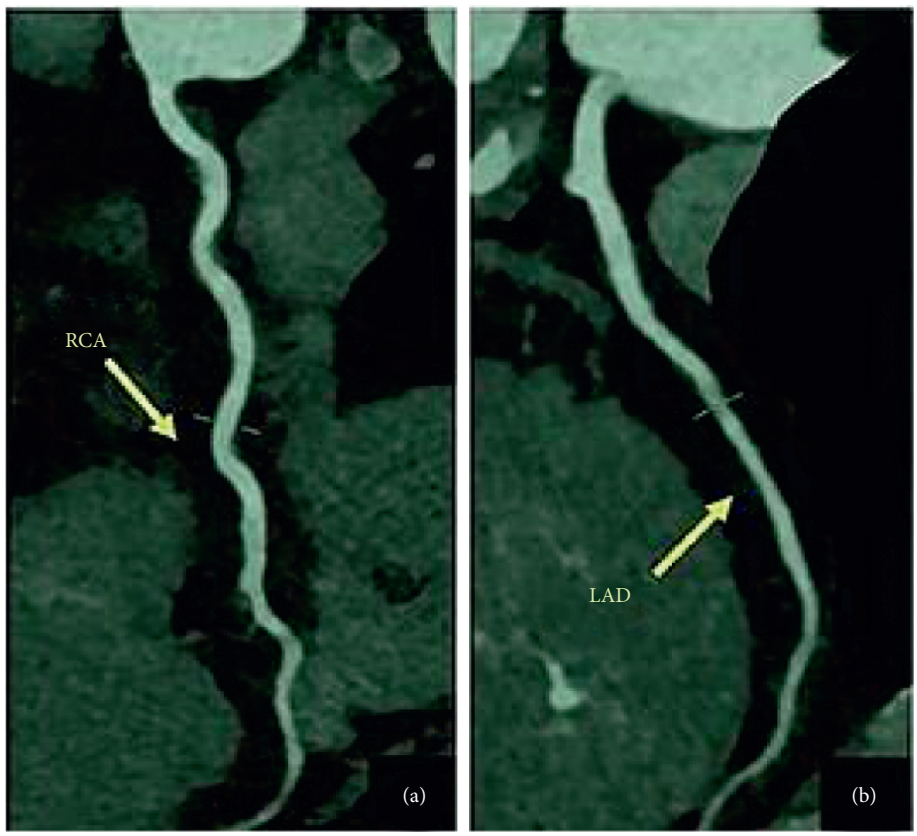

Figure 13: Extended CPR images of RCA and LAD. *Note.* A represents the extended CPR image corresponding to the center line RCA; B represents the extended CPR image corresponding to the center line LAD.

eliminate most of the branches, but there are still a few that cannot be completely eliminated. Although some calcified lesions can be detected and removed, there are still undetectable phenomena for small calcifications, and there is no way to distinguish stents from calcifications. However, there is a linear relationship between the change range of the area curve and the thickness of the lumen, which can be used to evaluate the stenosis degree of blood vessels. Through the implementation of extended CPR, it can be concluded from Figure 13 that LAD contains calcified plaque, and the symmetrical part can be observed in the figure, which is mainly determined by the extended reconstructed image. When people observe that the center line rises before the horizontal line along the observation direction, the symmetrical structure will be displayed in the resulting image. This symmetrical structure exists on the left and right and occurs at the lowest position of the bending part. In the implementation of straightened CPR, it can be concluded that the blood vessels in the straightening diagram in Figure 14 are not completely in the center of the image, which may be caused by the calculation error of the center line. Calcified plaques can be observed near the 380th floor in the

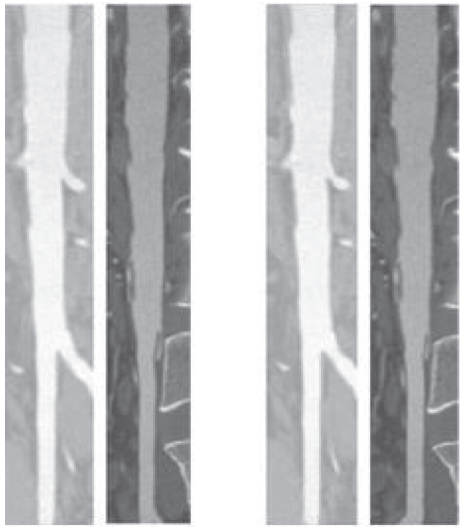

Figure 14: Straightened results at different angles by LAD.

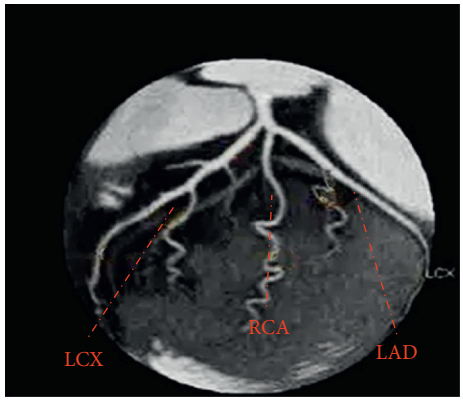

Figure 15: The three main coronary arteries and the fitted real mode sphere.

straightening diagram. As shown in Figure 15, during the realization of spherical CPR, the images had overlapping problems, and the blood vessels appeared in multiple layers in the radial direction. This may be because the spherical CPR maps the blood vessels to the curved surface in the radial direction. Then, the three visualization methods were compared. It was noted that extended CPR and straightened CPR had obvious advantages in displaying the local conditions of blood vessels, while spherical CPR had advantages in displaying the overall direction of blood vessels.

5. Conclusion

In the study, the CT images of coronary arteries were segmented using a cylindrical model, and different realization methods of CPR visualization were discussed. It was proved that, in the precise segmentation under the cylinder model, redundant branches and calcified plaques can be effectively removed to make the segmentation of the vascular lumen more accurate, which was beneficial to the diagnosis and treatment of cardiovascular diseases. Among the three visualization methods, by comparing the advantages and disadvantages of different visualization methods, a spherical reconstruction visualization method was obtained, which made the display of blood vessels more accurate. However, some limitations in the study should be noted. Some branches and plaques cannot be cleaned up, which will affect the accuracy of diagnosis to a certain extent. Therefore, in the follow-up study, these issues need to be resolved to achieve the best results.

Data Availability

The data used to support the findings of this study are available from the author upon request.

Conflicts of Interest

The author declares that there are no conflicts of interest.

References

[1] M. Zhou, H. Wang, X. Zeng et al., "Mortality, morbidity, and risk factors in China and its provinces, 1990-2017: a systematic analysis for the global burden of disease study 2017," *The Lancet*, vol. 394, no. 10204, pp. 1145–1158, 2019.

[2] S. T. Hu, R. L. Gao, and W. Wang, "The reach of the state in gao village," *Gao Village Revisited*, vol. 34, no. 03, pp. 209–220, 2019.

[3] C. Guo, J. Lu, Z. Tian, W. Guo, and A. Darvishan, "Optimization of critical parameters of PEM fuel cell using TLBO-DE based on Elman neural network," *Energy Conversion and Management*, vol. 183, pp. 149–158, 2019.

[4] O. Ronneberger, P. Fischer, and T. Brox, "U-net: convolutional networks for biomedical image segmentation," *Lecture Notes in Computer Science*, vol. 9351, pp. 234–241, 2015.

[5] Ö Çiçek, A. Abdulkadir, and S. S. Lienkamp, "3D U-net: learning dense volumetric segmentation from sparse annotation," in *Proceedings of the International Conference on Medical Image Computing and Computer-Assisted Intervention, MICCAI*, Athens, Greece, 2016 August.

[6] Z. Lv and W. Xiu, "Interaction of edge-cloud computing based on SDN and NFV for next generation IoT," *IEEE Internet of Things Journal*, vol. 7, no. 7, pp. 5706–5712, 2020.

[7] T. Buelow, R. Wiemker, T. Blaffert, C. Lorenz, and S. Renisch, "Automatic extraction of the pulmonary artery tree from multi-slice CT data," *Proceedings of SPIE: Medical Imaging*, vol. 5746, pp. 730–740, 2005.

[8] J. Leipsic, S. Abbara, S. Achenbach et al., "SCCT guidelines for the interpretation and reporting of coronary CT angiography: a report of the Society of Cardiovascular Computed Tomography Guidelines Committee," *Journal of Cardiovascular Computed Tomography*, vol. 8, no. 5, pp. 342–358, 2014.

[9] J. L. Li, Y. L. Huang, and D. Han, "Accuracy of artificial intelligence in the diagnosis of coronary heart disease in coronary CT angiography. Medical imaging technology in China," *Coronary Artery Disease (CAD)*, vol. 37, no. 1, pp. 59–62, 2021.

[10] L. D. Wan and H. H. Wu, "Application status of digital virtual human anatomy teaching platform," *Chinese Journal of histochemistry and Cytochemistry*, vol. 26, no. 6, pp. 625–628, 2017.

[11] T. Sun and S. Q. Han, "Application of 3D visualization in precise surgery of pancreatic tumor," *Journal of Medical Imaging*, vol. 29, no. 1, pp. 93–96, 2019.

[12] F. Jiang, Q. Gu, and N. Li, "Survey of content-based image segmentation methods," *Journal of Software*, vol. 28, no. 1, pp. 160–183, 2017.
[13] R. T. Farouki, "Rational rotation-minimizing frames-Recent advances and open problems," *Applied Mathematics and Computation*, vol. 272, pp. 80–91, 2016.
[14] Q. J. Zhang and X. M. Zhang, "Application of coronary CTA in clinical diagnosis of coronary heart disease," *Clinical medicine research and Practice*, vol. 16, pp. 158-159, 2017.
[15] S. Guo, R. Chen, H. Li, T. Zhang, and Y. Liu, "Identify severity bug report with distribution imbalance by CR-SMOTE and ELM," *International Journal of Software Engineering and Knowledge Engineering*, vol. 29, no. 2, pp. 139–175, 2019.
[16] E. Yaprak and S. Kayaalti-Yuksek, "Preliminary evaluation of near-infrared vein visualization technology in the screening of palatal blood vessels," *Medicina Oral, Patologia Oral Y Cirugia Bucal*, vol. 23, no. 1, pp. e98–e104, 2018.
[17] Y. Z. Xia, "Application of visualization in neurosurgery clinical practice teaching under new situation," *BMC Medical Education*, vol. 24, pp. 144-145, 2016.
[18] S. K. Yue, *Three-dimensional Modeling and Hemodynamics of Coronary Artery*, Jilin university, Changchun, China, 2017.
[19] Y. L. Guo, H. Y. Huang, and C. Y. Zhong, "Application of 3D visualization model of human coronary artery in diagnosis of coronary heart disease by transthoracic real-time 3D echocardiography," *China Digital Medicine*, vol. 6, no. 12, pp. 30–34, 2011.